Citation: Barhm Mohamad. Improving heat transfer performance of flat plate water solar collectors using nanofluids. *Journal of Harbin Institute of Technology (New Series)*. DOI:10.11916/j.issn.1005-9113.2024001.

Improving Heat Transfer Performance of Flat Plate Water Solar Collectors Using Nanofluids

Barhm Mohamad

(*Department of Petroleum Technology, Koya Technical Institute, Erbil Polytechnic University, Erbil 44001, Iraq*)

Abstract: This study delves into both experimental and analytical examinations of heat exchange in a straight channel, where Al_2O_3-water nanofluids are utilized, spanning the Reynolds number spectrum from 100 to 1800. Diverse volume fractions (1%, 2%, and 3%) of Al_2O_3-water nanofluids are meticulously prepared and analyzed. The essential physical properties of these nanofluids, critical for evaluating their thermal and flow characteristics, have been comprehensively assessed. From a quantitative perspective, numerical simulations are employed to predict the Nusselt number (Nu) and friction factor (f). The empirical findings reveal intriguing trends: the friction factor experiences an upward trend with diminishing velocity, attributed to heightened molecular cohesion. Conversely, the friction factor demonstrates a decline with diminishing volume fractions, a consequence of reduced particle size. Both the nanofluid's viscosity and heat transfer coefficient exhibit a rise in tandem with augmented volume flow rate and concentration gradient. Notably, the simulation results harmonize remarkably well with experimental data. Rigorous validation against prior studies underscores the robust consistency of these outcomes. In the pursuit of augmenting heat transfer, a volume fraction of 3% emerges as particularly influential, yielding an impressive 53.8% enhancement. Minor increments in the friction factor, while present, prove negligible and can be safely overlooked.

Keywords: Nusselt number; friction factor; nanofluids; flat plate solar collectors; solar energy

CLC number: TK513.1 **Document code**: A **Article ID**: 1005-9113(2024)00-0000-10

0 Introduction

Renewable energy emerges as a superior solution to the challenges of energy depletion, owing to its abundant availability and eco-friendly nature. Notably, solar water heater collectors stand out as a pivotal application of solar energy. These collectors serve the purpose of directly harnessing solar radiation and converting it into usable heat or electricity, finding applications across various industrial sectors. Engineered to harness sunlight's heat-absorbing potential, these collector systems play a crucial role in transforming solar energy into practical forms.

Defined as the component responsible for converting solar energy into diverse usable forms, the solar collector captures electromagnetic radiation across a spectrum, ranging from infrared to long-range ultraviolet (UV), with a visible solar energy component constituting 49%[1-3]. Enter nanofluids-dispersions of nanomaterials possessing enhanced properties. These nanofluids find extensive utility in diverse manufacturing contexts, including vehicle cooling, solar energy systems, and heat exchangers, thanks to their distinctive thermal attributes.

However, integrating nanoparticles into nanofluids introduces concerns, primarily surrounding nanoparticle stability within the base fluid. The interactions between nanoparticles and the overall stability of the nanofluid warrant thorough examination.

Previous research has explored the use of alumina nanoparticles at concentrations of 1%-3% mixed with water in laminar flow scenarios. Surface temperatures and pressure differentials across the test section were measured, revealing a notable increase in numerical values: 12%, 14%, and 16% enhancement in numbers correlating with nanofluid concentration and Reynolds number, respectively. This suggests that nanofluids have the potential to bolster the efficiency

Received 2023-01-04.

* Corresponding author: Barhm Mohamad, Ph.D, Lecturer. Email: barhm.mohamad@epu.edu.iq.

of solar collector systems[4].

Numerous researchers have delved into enhancing solar thermal efficiency through nanofluid integration. Their findings underscore that incorporating nanofluids into solar collectors leads to a 10% efficiency enhancement when compared to conventional fluids[5-6]. Further investigations highlight the impact of nanofluids on direct solar energy absorption by nanoparticles suspended in water. Carbon nanotubes increase efficiency by 5%, while copper particles boost it by 8%[7-8].

Tian et al.[1] used Artificial Neural Network (ANN) to analyze the effect of temperature and nanoparticle volume fraction on the thermal conductivity of Graphene oxide-Al2O3/Water-Ethylene glycol hybrid nanofluid. Nanofluids were prepared with varying nanoparticle volume fractions (0.1% to 1.6%) and temperatures (25 - 55°C). The ANN was effectively trained to predict thermal conductivity, yielding an average MSE of 1.67e-6 and a correlation coefficient of 0.999. Results indicated that nanoparticle volume fraction had a more significant impact on thermal conductivity compared to temperature, especially at low concentrations. At high concentrations, increasing temperature led to a further increase in thermal conductivity. For instance, at a volume fraction of 1.6%, increasing temperature from 20° C to 55° C raised thermal conductivity from 0.45 W/mK to 0.54 W/mK. The study underscores the crucial role of nanoparticle volume fraction in enhancing thermal conductivity in hybrid nanofluids. Applying nanofluids within heat exchangers has been shown to optimize system performance, validated through extensive research[9-12]. Notably, Mohammed et al.[13] conducted a theoretical exploration of heat transfer improvements facilitated by various nanofluids, including silver, alumina, titanium, and silica. Their study yielded a substantial 15% increase in the performance factor.

In a holistic context, Khodabandeh et al.[14] conducted a numerical investigation on laminar water nanofluid flow containing GNP-SDBS nanoparticles. The study explored mass fractions of solid nanoparticles from 0 to 0.1% and Reynolds numbers from 50 to 1000 using the finite volume method. They proposed a novel microchannel design where countercurrent flow was employed in upper and lower layers, with enhanced mixing facilitated by cavities, sinusoidal routes, and rectangular ribs on microchannel walls. Results showed a 20% increase in average Nusselt number for each Reynolds number considered, alongside improved heat transfer efficiency and temperature uniformity, especially in the lower layer. The recommended microchannel design is suggested for Reynolds numbers less than 300 to optimize heat transfer. The research conducted by Al-Kouz et al.[15] explored the performance analysis of an electrically conducting water-Fe3O4/CNT hybrid nanofluid within a trapezoidal enclosure with wavy walls. Using computational methods, the study investigated three-dimensional free convection and entropy generation, taking into account a hybrid nanoliquid layer and a permeable medium layer within the enclosure. Various parameters, including the Darcy number, Hartmann number, volume fraction, undulation number of the wavy wall, and Rayleigh number, were considered in the analysis. By employing the Galerkin finite element method through COMSOL Multiphysics software, the researchers analyzed the effects of these parameters on streamlines, isotherms, and Bejan number contours. Notably, an increase in Hartmann and Rayleigh numbers was found to significantly reduce the average Bejan number, whereas the average Nusselt number decreased notably only at very high Rayleigh and high Hartmann numbers. The study also observed that increasing the undulation number led to a substantial elevation of the average Nusselt number, particularly at very high Rayleigh numbers. Conversely, an increase in the Darcy number was associated with a significant increase in the average Nusselt number while reducing the average Bejan number. These findings have implications for various applications, including hybrid magnetic nanofluid fuel cells and the processing of electromagnetic nanomaterials in cavities, offering insights into thermal flow characteristics and performance under complex conditions involving magnetic fields, porous media, and thermal buoyancy. The main objective of this research work is to investigate heat exchange in a straight channel using Al_2O_3-water nanofluids across a range of Reynolds numbers (100 to 1800). The study involves both experimental and analytical approaches, including the preparation and analysis of nanofluids with varying volume fractions (1%, 2%, and 3%). The physical properties crucial for assessing thermal and flow characteristics are comprehensively evaluated. Numerical simulations are employed to

predict Nusselt number (Nu) and friction factor (f) quantitatively, adds a novel dimension to the investigation.

1 Preparation of Nanofluids

This paper explores the dispersion of Al_2O_3 nanoparticles within a base fluid (water) to create nanofluids. The calculation in Eq.(1) determines the necessary nanoparticle count to generate nanofluids at three volume fractions: 1%, 2%, and 3%. This methodology stands as the prevailing approach for nanofluid preparation, involving the introduction of nanoparticles into the fluid medium. To ensure even distribution and avert aggregation, an electric mixer is employed. Remarkably, an effective means of enhancing nanofluids' physical properties involves reducing the surface tension of the dissolved warm liquid, as elucidated by Ref. [15].

The nanofluids, comprising Al_2O_3 particles within water, are formulated at distinct concentrations: 1%, 2%, and 3% by volume. Each nanofluid concentration is combined with 10 L of water. Fig. 1 visually portrays nanofluid samples showcasing varying concentrations. Notably, the prepared nanofluids (Al_2O_3/water) exhibit stability across all tests . It is noteworthy that no surfactants, which could potentially alter the nanoparticles' physical properties, were introduced into the nanofluid mixture. The quantity of particles required for nanofluid preparation can be determined using the subsequent relationship[16]:

$$\varphi = \frac{\dfrac{m_p}{\rho_p}}{\dfrac{m_p}{\rho_p} + \dfrac{m_f}{\rho_f}} \tag{1}$$

Where φ represents the volume fractions of (Al_2O_3/water); m_p represents the mass of the Al_2O_3; ρ_p is the density of Al_2O_3; mf represents the mass of the water; ρ_f is the density of water. Table 1 provides an overview of the physical properties of both water and nanofluids mixture at different volume fractions.

Fig.1 Samples of nanofluid

Table 1 The physical properties of water and nanofluids mixture

Volume fractions φ (%)	Thermal conductivity (W·m^{-1}·K^{-1})	Specific heat (J·kg^{-1}·K^{-1})	Viscosity (N·m^{-2}·s)	Density (kg·m^{-3})
0	0.6000	4181	0.001008	1000
1	0.6279	4146.84	0.001100	1026
2	0.6458	4112.68	0.001108	1052
3	0.6641	4078.52	0.001110	1078

1.1 Experimental Setup

Illustrated in Fig. 2 are the apparatuses employed for assessing convection characteristics and pressure drop within a straight channel using nanofluids. Commencing with the lowest flow rate, a state of data stability is initially established. Subsequently, a modest increase in the volume flow rate prompts the system to reattain equilibrium. Maintaining a constant input temperature, the experimental setup necessitates approximately 18 to 25 min to restore stability subsequent to the rise in volume flow rate. Upon achieving the input temperature once more, data collection is reiterated. This procedural iteration persists until the maximum flow rate is attained. In a similar vein, alterations in the volume concentrations of nanofluids are introduced, followed by the replication of the aforementioned actions.

1.2 Empirical Method and Theoretical Evaluation

The empirical configuration of the present study is elucidated in Fig.2. The setup primarily comprises essential components such as thermocouples, a flow meter, a manometer, a pump, and the test section. To propel the nanofluid through the test section, a 370 W pump exerts force, drawing the fluid from a 10 L reservoir. The upper and lower walls of the rig are subjected to solar irradiation and are effectively insulated. Ensuring minimal heat exchange with the

environment, the test section is enveloped by 5 cm thick layers of fiberglass insulation. Within the fluid circulation path, a flow meter is integrated, positioned between the circulation pump and the entry point of the development section. This flow meter boasts the capacity to accurately gauge flow rates ranging from 10 to 110 cubic centimeters per minute (CCPM).

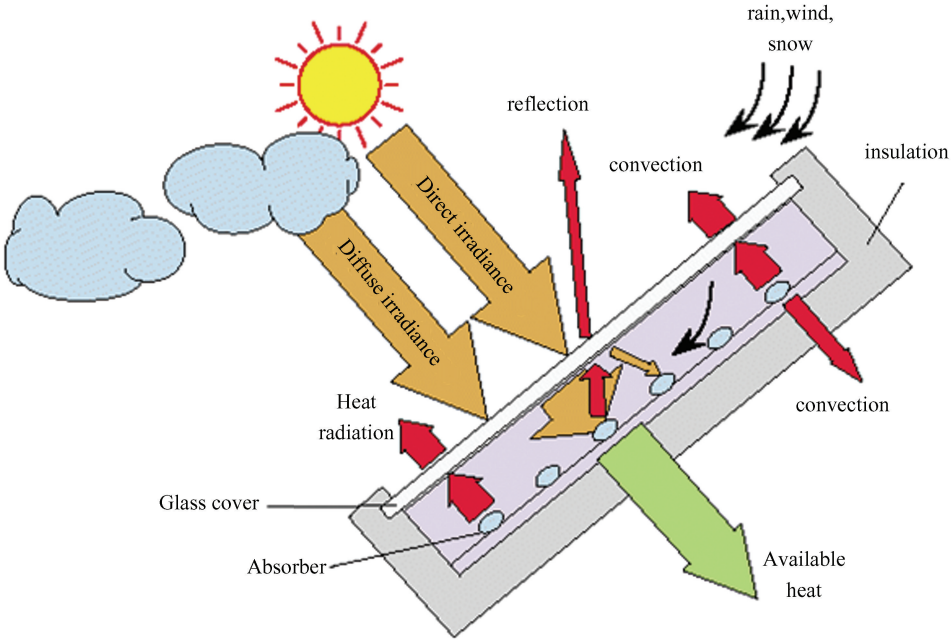

Fig.2 A diagrammatic representation of the experimental set-up

1.3 Correlation of Data

The quantification of heat absorbed by the nanofluids from the test area can be determined employing the following formula[17-19]:

$$Q_u = \dot{m}\,\mathrm{Cp}_w(T_{\mathrm{ws.co}} - T_{\mathrm{ws.cin}}) \tag{2}$$

where: $m^{\cdot}$ is fluid mass flow rate, Cp_w is fluid specific heat, $T_{\mathrm{ws.cin}}$ and $T_{\mathrm{ws.co}}$ are fluid inlet to the solar collector and fluid outlet from the solar collector.

To delineate the average heat transfer coefficient, one can utilize the following expression[18]:

$$h_{nf} = \frac{\mathrm{Cp}_{nf} \cdot \rho_{nf} \cdot U \cdot A(T_{\mathrm{out}} - T_{\mathrm{in}})}{\pi \cdot D \cdot L(T_s - T_b)} \tag{3}$$

where h_{nf} represents the convective heat transfer coefficient of a nanofluid flowing inside a tube, Cp_{nf} is the specific heat capacity of the nanofluid, ρ_{nf} is the density of the nanofluid, U The average velocity of the nanofluid flow, Ac is the cross-sectional area of the tube, T_{out}, T_{in} are the outlet and inlet temperatures of the nanofluid, respectively, D is the inner diameter of the tube, L is the length of the tube in meters. Finally, T_s represents the surface temperature of the tube wall, and T_b is the bulk mean temperature of the nanofluid. The formula for computing the average Nusselt number is presented below[18]:

$$\mathrm{Nu}_{nf} = \frac{h_{nf} \times D_h}{k_{nf}} \tag{4}$$

In above equation, k_{nf} represents the fluid's ability to conduct heat and D_h stands for the hydraulic diameter of a straight channel which is describe as below[18]:

$$D_h = \frac{4A_c}{Pm} \tag{5}$$

where Pm is the wetted perimeter, defined as the total length of all sides in contact with the fluid for a non-circular conduit. The expression for the frication factor (f) [20]:

$$f = \frac{\dfrac{2 \times \triangle P}{\dfrac{L}{D} \times \rho \times U_{\mathrm{in}}^2}}{4} \tag{6}$$

where $\triangle P$ is the pressure drop across the length of the pipe, U_{in} represents the average inlet velocity of the fluid. the The Nusselt number, serving as an indicator of the heat transfer coefficient, quantifies the heat transferred within a system. The Nusselt number, serving as an indicator of the heat transfer coefficient, quantifies the heat transferred within a system. In the context of laminar flow, the Shah-London equation is

employed to characterize this phenomenon[21].

$$\mathrm{Nu}_{av} = 1.953\left[\mathrm{Re}\cdot D_h P_r \frac{D_h}{L}\right]^{\frac{1}{3}} \quad (7)$$

where R_e and P_r are the Reynolds number and Prandtl number, respectively.

2 Mathematical Formulation

2.1 Problem Description

As illustrated in Fig. 3, the current investigation employs straight channels as the software setup. These channels are characterized by walls on both the upper and lower surfaces, uniformly subjected to heat flux conditions. The assumptions governing this study encompass a steady and developed flow, characterized by two - dimensional movement and incompressibility. Additionally, the nanofluid mixture (Water/Al_2O_3) is presumed to be in a state of thermal equilibrium and experiences consistent flow velocity. Furthermore, the mixture is assumed to exhibit Newtonian fluid behavior.

2.2 Management Equations

The non-dimensional governing equations for a nanoparticle-based fluid mixture that has laminar flow, are non-compressible, homogeneous and stable in two dimensions[19]:

Continuity equation:

$$\frac{\partial U}{\partial X} + \frac{\partial U}{\partial Y} = 0 \quad (8)$$

U-momentum equation:

$$\left(U\frac{\partial U}{\partial X} + V\frac{\partial V}{\partial Y}\right) = -\frac{\mathrm{d}p}{\mathrm{d}X} + \frac{1}{\mathrm{Re}}\left(\frac{\partial^2 U}{\partial X^2} + \frac{\partial^2 U}{\partial Y^2}\right) \quad (9)$$

V-momentum equation:

$$\left(U\frac{\partial V}{\partial X} + V\frac{\partial V}{\partial Y}\right) = -\frac{\mathrm{d}p}{\mathrm{d}Y} + \frac{1}{\mathrm{Re}}\left(\frac{\partial^2 V}{\partial X^2} + \frac{\partial^2 V}{\partial Y^2}\right) \quad (10)$$

Energy equation:

$$\left(U\frac{\partial \theta}{\partial X} + V\frac{\partial \theta}{\partial Y}\right) = \frac{1}{\mathrm{Re}\cdot pr}\left(\frac{\partial^2 \theta}{\partial X^2} + \frac{\partial^2 \theta}{\partial Y^2}\right) \quad (11)$$

2.3 Grid Independent Test

In a broader sense, the credibility of numerical calculations hinges on the grid independence test, which determines the requisite grid size for the present investigation. This test was executed across four distinct grid dimensions (9.6×23, 23×26, 15×47, 20×100). Utilizing these grid sizes, the Nusselt number(Nu) and the distribution of the friction factor (f) were computed along the walls of a straight channel containing AL_2O_3-nanofluids. This calculation encompassed three different volume fractions, with Reynolds numbers ranging from 100 to 1800, and maintained a consistent length (25 cm) and width (2.5 cm) of the channel.

2.3.1 *Geometrical model*

The geometry was implemented based on the current Flat Plate Solar Collector (FPSC) prototype using OpenFOAM toolbox advanced design software, including the absorber plate, tubes, cover the glass, the air space between the glass and the absorber plate. The cross section details were explained in Fig. 3.

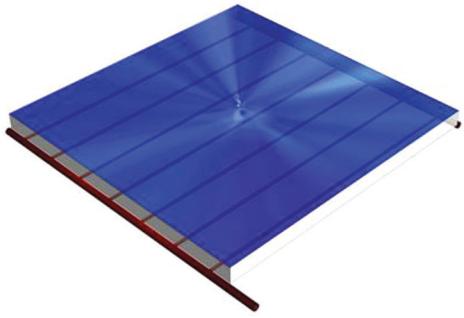

Fig. 3 The absorber of FPSC

2.3.2 *Mesh generation*

Conducting grid-independent tests aids in striking a balance between accuracy and computational efficiency. The number of elements directly impacts the computational time required. In this model, the output entails 1.5 million cells. Fig. 4 illustrates the condition of the mesh, highlighting the identified exposed zones.

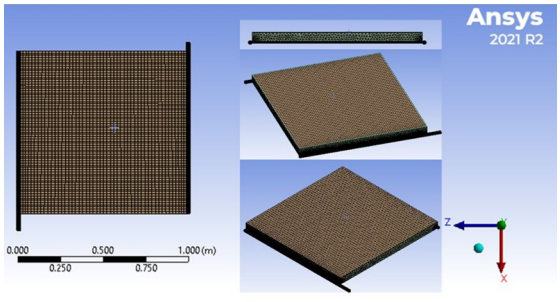

Fig. 4 Refinement mesh of FPSC and tubes

The sizing reached a maximum of 0.14962 m, alongside high smoothing settings. A total of 330910 statistics nodes and 1416020 elements were employed, with five layers of inflation featuring smooth transitions. The change ratio stood at 0.272, while the growth rate was 1.2. The setup incorporated physical properties pertaining to glass, aluminum,

copper, air, and established boundary conditions for the flat solar collector. Positions and flow rates for the collectors were determined. To theoretically compute the glazing absorption plate's temperature, the solver employed continuity, momentum, and energy conservation equations. Boundary conditions were specified for particles smaller than 20 nm, assuming a spherical shape, density of 3510 kg/m^3, conductivity of 1000 W/(m·K), and specific heat of 497.26 J/(kg·K). Nanofluid thermophysical properties were automatically updated by the solver. Its primary objective was to assess the thermal performance of the FPSC. Results from the software's post-processing are depicted in Fig. 5.

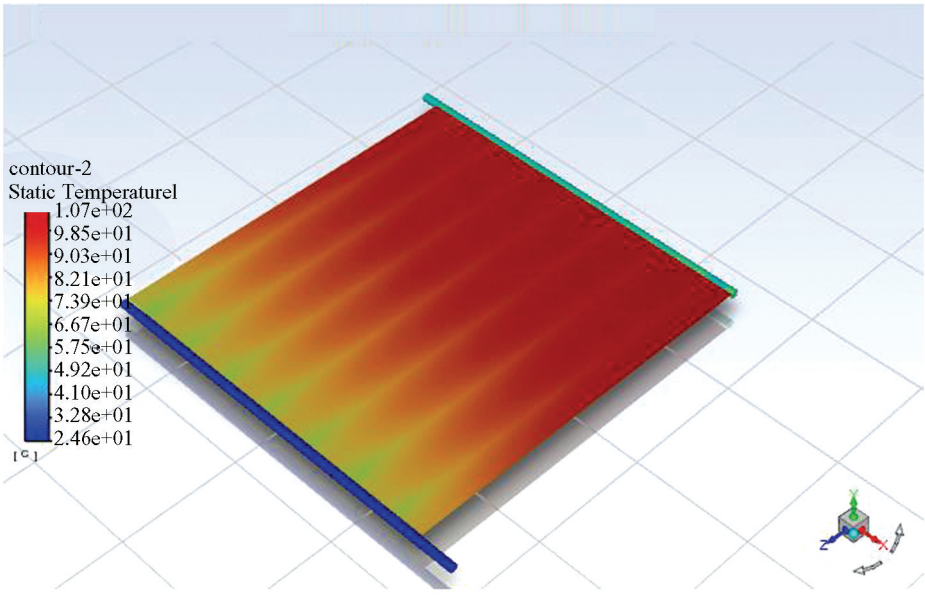

(a) The temperature distribution across both the absorbent plate and the tube

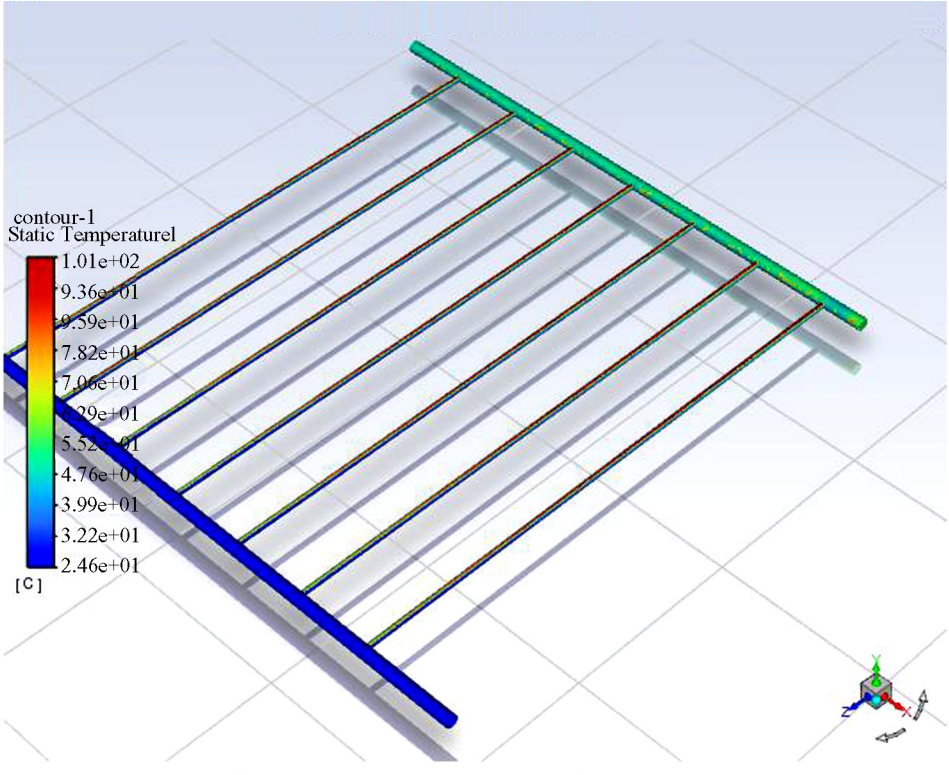

(b) The temperature distribution along the tubes and headers

Fig. 5 The physical contours of the Flat Plate Solar Collector (FPSC)

The Nusselt number appears to increase slightly with a significant rise in Reynolds numbers across various grid dimensions, as shown in Fig. 6(a). The friction factor exhibits a decreasing trend with increasing Reynolds numbers across various grid dimensions. This implies that, for different grid sizes, the friction factor tends to decrease as the Reynolds number increases, as shown in Fig. 6(b).

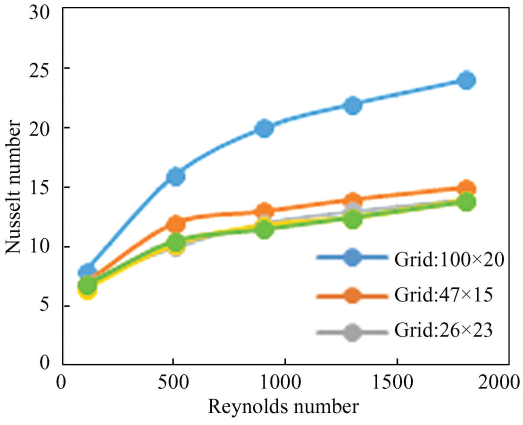

(a) Nusselt number trends with Reynolds number and grid sizes

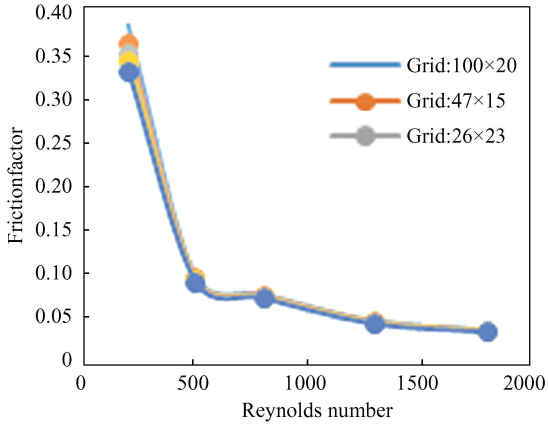

(b) Friction factor trends across varying grid sizes

Fig. 6 Grid independence test at different Reynolds numbers

2.4 Validation of Numerical Methods

In an endeavor to affirm the accuracy of both numerical analysis and empirical findings, several metrics were scrutinized: the Nusselt number, friction factor, relative thermal conductivity, and relative viscosity. These metrics were juxtaposed with the simulation results derived from earlier studies. Notably, the average Nusselt number concerning the laminar flow of nanofluids between parallel plates was calculated and contrasted against outcomes from prior numerical investigations[22-25].

The trends that emerged from this comparison were intriguing. Fig. 7(a) visually underscores the Nusselt number's correlation with Reynolds number, revealing that an increase in the latter corresponds to a rise in the former. Meanwhile, the simulation outcomes of the friction factor were aligned with those reported in other relevant literature[26-33]. This alignment led to the deduction that the friction factor escalates as the size of nanoparticles decreases, as visually depicted in Fig.7(b).

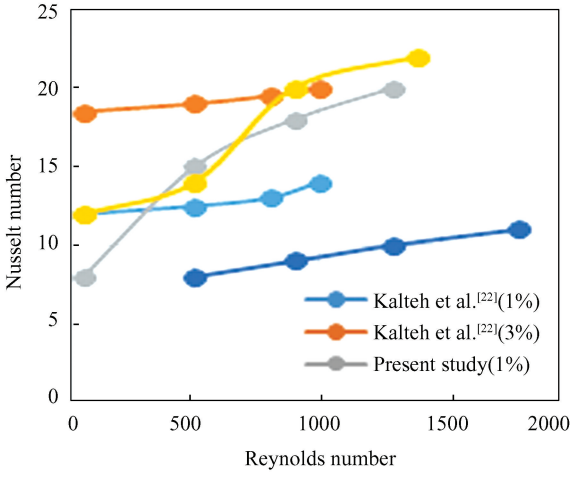

(a) Correlation between Nusselt number and Reynolds number

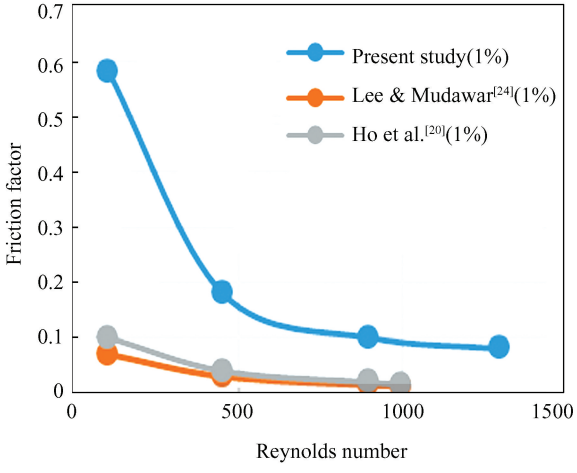

(b) Correlation between friction factor and Reynolds number

Fig. 7 Validation of Nusselt number and friction factor

3 Results and Discussions

3.1 Nusselt Number

The interplay between the Nusselt number and Reynolds number is vividly depicted in Fig. 8, considering nanofluids at varying velocities (6−15 mm/s) and nanoparticle diameters (30 nm). In the experimental examination of a straight channel, it becomes evident that the Nusselt number increases in direct proportion to the velocity surge, attributed to the concurrent escalation of Reynolds number. This correlation is observable.

Interestingly, when nanoparticles' size is amplified, an observable elevation in the Nusselt number occurs for a given Reynolds number. This trend aligns with expectations and demonstrates the impact of particle size on heat transfer dynamics. Additionally, the modest increase in thermal conductivity for the liquid contributes to a corresponding rise in the rate of heat transfer, aligning with predictions made by other researchers[31].

It is worth noting that among the considered fluids, pure water ($\emptyset$ = 0%) exhibits the lowest Nusselt number. This disparity can be attributed to its comparably lower thermal conductivity compared to nanofluids, further emphasizing the beneficial effects of nanoparticle dispersion on heat transfer efficiency.

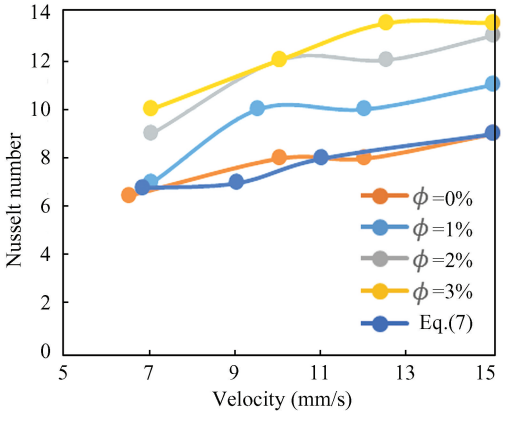

Fig. 8 Empirical results of Nusselt number

3.2 Friction Factor

The friction factor, as illustrated in Fig. 9, spans a range from 7 mm/s to 15 mm/s, providing a clear demonstration of the significant interplay between the friction factor (f) and the Reynolds number (Re). Notably, as the velocity of nanofluid particles increases, there is a distinct reduction in the friction factor. In contrast, a noticeable upward trend in the friction factor becomes apparent with escalating volume concentrations of substances.

These trends are deeply influenced by the viscosity characteristics of the nanofluids. This viscosity influence leads to heightened friction factors within the channel, a phenomenon intriguingly aligned with the observations of previous researchers who faced challenges in conclusively establishing this relationship[32]. This harmony in findings reinforces the paramount importance of comprehending the intricate connection between nanofluid viscosity and the behavior of the friction factor within the channel.

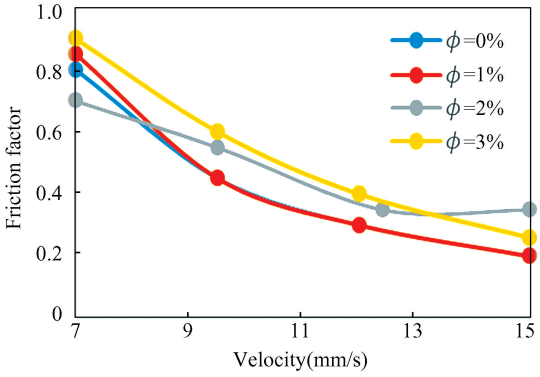

Fig. 9 Empirical results of friction factor

4 Conclusions

In the realm of nanotechnology, the fabrication of nanoparticles has reached remarkable heights in contemporary times. Among their diverse applications, nanofluids hold a crucial role in enhancing heat transfer processes. These fluids introduce a new dimension by infusing conventional water with nanoparticles, thereby yielding a novel medium for effective heat transfer. This article provides an encompassing overview of recent strides in harnessing nanostructures to investigate heat transfer dynamics in solar collectors.

Nanofluids, comprising minute nanoparticle quantities, exhibit significantly heightened thermal conductivity compared to regular water. Essential factors, including particle size, nanoparticle composition, and the underlying material, intricately influence the heat transmission capacity of these fluids. The presence of these exceptional nanoparticles tangibly augments the heat transfer efficiency of the fluid involved in convection processes.

The impact of nanofluids' additives on overall solar system efficiency has been systematically evaluated. During experimental trials, the concentration of nanofluids proved to significantly influence the efficiency of solar collectors. This influence extended to parameters such as friction coefficient and Nusselt number, which were meticulously correlated through adept correlation equations. Moreover, input coefficients, including Reynolds number and nanoparticle size concentrations, were explored under flux conditions. Intriguing findings emerged from these computations. The authors substantiated that as the Reynolds number decreases, the coefficient of friction factor increases. Simultaneously, the coefficient of heat transmission exhibits an increment as both Reynolds number and particle size increase. This interplay underscores the intricate relationship between fluid dynamics, nanoparticle characteristics, and heat transfer efficiencies.

References

[1] Tian S P, Arshad N I, Toghraie D, et al. Using perceptron feed-forward Artificial Neural Network (ANN) for predicting the thermal conductivity of graphene oxide-Al2O3/water - ethylene glycol hybrid nanofluid. Case Studies in Thermal Engineering, 2021, 26: 101055. DOI: 10.1016/j.csite.2021.101055.

[2] Ahmed S T, Ali H H M. Experimental investigation of new design of solar water distillation coupled with flat plate solar water collector. The Iraqi Journal for Mechanical and Material Engineering, 2020, 20(3): 193-207. DOI: 10.32852/iqjfmme.v20i3.512.

[3] Javadi F S, Saidur R, Kamalisarvestani M. Investigating performance improvement of solar collectors by using nanofluids. Renewable and Sustainable Energy Reviews, 2013, 28: 232-245. DOI: 10.1016/j.rser.2013.06.053.

[4] Hossein C, Yahya A, Esmaeil E, et al. Experimental study on thermal efficiency of flat plate solar collector using TiO2/water nanofluid. Modern Applied Science, 2013, 7(10): 60-69. DOI: 10.5539/mas.v7n10p60.

[5] Zhongyang L, Cheng W, Wei W, et al. Performance improvement of a nanofluid solar collector based on direct absorption collection (DAC) concepts. International Journal of Heat and Mass Transfer, 2014, 75: 262-271. DOI: 10.1016/j.ijheatmasstransfer.2014.03.072.

[6] Faizal M, Saidur R, Mekhilef S, et al. Energy, economic and environmental analysis of metal oxides nanofluid for flat - plate solar collector. Energy Conversion and Management, 2013, 76: 162 - 168. DOI: 10. 1016/j.enconman.2013.07.038.

[7] Otanicar T P, Phelan P E, Prasher R S, et al. Nanofluid based direct absorption solar collector. Journal of Renewable and Sustainable Energy, 2010, 2: 033102. DOI: 10.1063/1.3429737.

[8] Menni Y, Chamkha A, Lorenzini G, et al. Advances of nanofluids in solar collectors - A review of numerical studies. Mathematical Modelling of Engineering Problems, 2019, 6(3): 415-427. https://doi.org/10.18280/mmep.060313.

[9] Jaafar A, Satinder T, Mushtaq A. Heat transfer through heat exchanger using Al_2O_3 nanofluid at different concentrations. Case Studies in Thermal Engineering, 2013, 1(1): 38-44. DOI: 10.1016/j.csite.2013.08.004.

[10] Reza A, Heydar M, Malihe Z, et al. Heat transfer of nanofluid in a double pipe heat exchanger. International Scholarly Research Notices, 2014, Article ID: 736424. DOI: 10.1155/2014/736424.

[11] Gabriela H, Angel H. Application of nanofluids in heat exchangers: A review. Renewable and Sustainable Energy Reviews, 2012, 16: 5625-5638. DOI: 10.1016/j.rser.2012.05.023.

[12] Kumar V, Tiwari A K, Ghosh S K. Characterization and Performance of Nanofluids in Plate Heat Exchanger." Materials Today: Proceedings, 2017, 4(2), Part A, pp. 4070-4078. DOI: 10.1016/j.matpr.2017.02.310

[13] Mohammed H A, Bhaskaran G, Shuaib N H, et al. Numerical study of heat transfer enhancement of counter nanofluids flow in rectangular microchannel heat exchanger. Superlattices and Microstructures, 2011, 50(3): 215-233. DOI: 10.1016/j.spmi.2011.06.003.

[14] Khodabandeh E, Rozati S A, Joshaghani M, et al. Thermal performance improvement in water nanofluid/GNP - SDBS in novel design of double - layer microchannel heat sink with sinusoidal cavities and rectangular ribs. Journal of Thermal Analysis and Calorimetry, 2019, 136: 1333 - 1345. DOI: 10. 1007/s10973-018-7826-2.

[15] Al-Kouz W, Abderrahmane A, Shamshuddin M D, et al. Heat transfer and entropy generation analysis of water-Fe3O4/CNT hybrid magnetic nanofluid flow in a trapezoidal wavy enclosure containing porous media with the Galerkin finite element method. The European Physical Journal Plus, 2021, 136: 1184. DOI: 10.1140/epjp/s13360-021-02192-3.

[16] Ramachandran K, Hussein A M, Kadirgama K, et al. Thermophysical properties measurement of nano cellulose in ethylene glycol/water. Applied Thermal Engineering, 2017, 123: 1158-1165. DOI: 10.1016/j.applthermaleng.2017.05.067.

[17] Hussein A M, Khaleell O S, Danook S H. Enhancement of double-pipe heat exchanger effectiveness by using water - CuO. NTU Journal of Engineering and Technology, 2022, 1(2): 18-22. DOI: 10.56286/ntujet.v1i2.59.

[18] Heydari M, Toghraie D, Akbari O A. The effect of semi-attached and offset mid-truncated ribs and Water/$T_i O_2$ nanofluid on flow and heat transfer properties in a triangular microchannel. Thermal Science and Engineering Progress, 2017, 2: 140-150. DOI: 10.1016/j.tsep.2017.05.010.

[19] Zarda F, Hussein A M, Danook A H, et al. Enhancement of thermal efficiency of nanofluid flows in a flat solar collector using CFD. Diagnostyka, 2022, 23(4): 2022411. DOI: 10.29354/diag/156384.

[20] Ho C J, Wei L C, Li Z W. An experimental investigation of forced convective cooling performance of a microchannel heat sink with Al_2O_3/water nanofluid. Applied Thermal Engineering, 2010, 30(2-3): 96-103. DOI: 10.1016/j.applthermaleng.2009.07.003

[21] Shah R K, London A L. Laminar Flow Forced Convection in Ducts: A Source Book for Compact Heat Exchanger Analytical Data. Amsterdam: Academic Press. 2014. DOI: 10.1016/C2013-0-06152-X.

[22] Kalteh M, Abbassi A, Saffar-Awal M, et al. Experimental and numerical investigation of nanofluid forced convection inside a wide microchannel heat sink. Applied Thermal Engineering, 2012, 36: 260e268. DOI: 10.1016/j.applthermaleng.2011.10.023.

[23] Ferroullit S, Bontemps A, Ribeiro J P, et al. Hydraulic and heat transfer study of SiO2/water nanofluids in horizontal tubes with imposed wall temperature boundary conditions. International Journal of Heat and Fluid Flow, 2011, 32(2): 424-439. DOI: 10.1016/j.ijheatfluidflow.2011.01.003.

[24] Lee J, Mudawar I. Assessment of the effectiveness of nanofluids for single-phase and two-phase heat transfer in micro - channels. International Journal of Heat Mass Transfer, 2007, 50(3-4): 452-463. DOI: 10.1016/j.ijheatmasstransfer.2006.08.001.

[25] Hussein A M, Sharma K V, Bakar R A, et al. A review of forced convection heat transfer enhancement and hydrodynamic characteristics of a nanofluid. Renewable and Sustainable Energy Reviews, 2014, 29: 734-743. DOI: 10.1016/j.rser.2013.08.014.

[26] Alina A M. Uncertainties in modeling thermal conductivity of laminar forced convection heat transfer with water alumina nanofluids. International Journal of Heat and Mass Transfer, 2014, 68: 78-84. DOI: 10.1016/j.ijheatmasstransfer.2013.09.018.

[27] Suhaib U I, Rajashekhar P, Narahari M. Engineering Applications of Nanotechnology. Topics in Mining, Metallurgy and Materials Engineering. Berlin: Springer. 2017. DOI: 10.1007/978-3-319-29761-3.

[28] Hussein A M, Sharma K V, Bakar R A, et al. The effect of nanofluid volume concentration on heat transfer and friction factor inside a horizontal tube. Journal of Nanomaterials, 2013, Article ID: 859563. DOI: 10.1155/2013/859563.

[29] Barnoon P, Toghraie D, Balali Dehkordi R, et al. Two phase natural convection and thermal radiation of Non-Newtonian nanofluid in a porous cavity considering inclined cavity and size of inside cylinders. International Communications in Heat and Mass Transfer, 2019, 108: 104285. DOI: 10.1016/j.icheatmasstransfer.2019.104285.

[30] Yan S R, Toghraie D, Abdulkareem L A, et al. The rheological behavior of MWCNTs-ZnO/Water-Ethylene glycol hybrid non-Newtonian nanofluid by using of an experimental investigation. Journal of Materials Research and Technology, 2020, 9(4): 8401-8406. DOI: 10.1016/j.jmrt.2020.05.018.

[31] Azeez K, Hameed A F, Hussein A M. Nanofluid heat transfer augmentation in a double pipe heat exchanger. AIP Conference Proceedings. New York: AIP Publishing LLC. 2020, 2213 (1): 020059. DOI: 10.1063/5.0000243.

[32] Hussein A M, Kadirgama K, Noor M M. Nanoparticles suspended in ethylene glycol thermal properties and applications: An overview. Renewable and Sustainable Energy Reviews, 2017, 69: 1324-1330. DOI: 10.1016/j.rser.2016.12.047.

[33] Kaska S A, Khalefa R A, Hussein A M. Hybrid nanofluid to enhance heat transfer under turbulent flow in a flat tube. Case Studies in Thermal Engineering, 2019, 13: 100398.DOI: 10.1016/j.csite.2019.100398.